Differential atomic magnetometry based on a diverging laser beam

E. Hodby,[a] E. A. Donley, and J. Kitching
Time and Frequency Division, National Institute of Standards and Technology, 325 Broadway, Boulder, Colorado 80305

(Received 30 April 2007; accepted 11 June 2007; published online 3 July 2007)

The authors demonstrate a novel atomic magnetometer that uses differential detection of the spatially diverging components of a light field to monitor the Larmor precession frequency of atoms in a thermal vapor. The design is implemented in compact form with a micromachined alkali vapor cell and a naturally divergent light field emitted by a vertical-cavity surface-emitting laser. Operating the magnetometer in differential mode cancels common-mode noise and improves the sensitivity by a factor of 26 over single-channel operation. They also suggest ways in which the current sensitivity of 28 pT/$\sqrt{}$Hz may be improved further without sacrificing size or simplicity.
 [DOI: 10.1063/1.2753763]

For the past 30 years, the field of sensitive dc magnetometry has been dominated by large, cryogenically cooled instruments based on superconducting quantum interference devices (SQUIDs).[1] Recently, atomic magnetometers,[2] which measure magnetic fields using optical pumping and probing of alkali atoms, have been developed whose sensitivities rival or even surpass[3] that of a typical SQUID. The lack of cryogenic cooling and the development of minute, easily tunable diode lasers make atomic magnetometers ideal candidates for miniaturization, with components fabricated by techniques commonly used in microelectromechanical systems (MEMS).[4] Since MEMS techniques are amenable to wafer-level fabrication, the potential exists for mass production of highly sensitive, low power (~1 mW), and low cost (~ few dollars) chip-scale magnetometers. Such devices would have a huge range of applications from mapping the magnetic fields of the heart and brain[5] to predicting earthquakes and measuring magnetic fields in space.[6]

This letter presents a new optical design for a chip-scale, differential magnetometer, and demonstrates, for the first time, common-mode noise rejection in a miniature physics package. The simplicity of the design, which uses just a single uncollimated beam from a vertical-cavity surface-emitting diode laser (VCSEL), makes it ideally suited for highly miniaturized chip-scale implementations and wafer-level mass production. Several aspects of the design are closely related to a miniature atomic clock recently developed at NIST.[7]

The experimental setup is shown in Fig. 1(a). At the heart of the apparatus is the miniature physics package shown in the inset of Fig. 1(a). The cell containing ^{87}Rb vapor is microfabricated by etching a 1 mm^2 hole in a 1 mm thick silicon wafer and sealed by anodically bonding glass wafers to either side.[8] It also contains a buffer gas mixture of Ar, Ne, and N_2 with pressures of 5, 31, and ~30 kPa at room temperature, respectively, which reduces the rate of decohering collisions ($1/T_2$) between Rb atoms and the cell walls. The cell is illuminated by a single VCSEL beam with an output power of 300 μW. (Note that the power reaching the photodiodes is only a few percent of this—the losses are due primarily to imperfect beam alignment and defects in the cell windows.) The laser is temperature tuned to the center of the collisionally broadened $D1$ absorption line (795 nm). The beam is uncollimated with a half-intensity, half-angle divergence of 3.8°. The strong central part of the beam is used for optically pumping the atoms while the diverging wings act as four probe beams, each of which is monitored by a 0.25 mm^2 segment of a quadrant photodiode mounted immediately above the cell. By using just a single laser beam to both pump and multiply probe the atoms, without collimating optics, beamsplitters, or mirrors, we are able to demonstrate a core physics assembly for the differential magnetometer with a volume of less than 1 cm^3. The temperatures of the cell and laser are held at 117 and 49 °C, respectively, by copper rods. The rods are heated by coils outside a single-layer magnetic shield, thus preventing magnetic fields generated by heating currents from perturbing the magnetometer. Nonmagnetic chip-scale heaters are being developed[4] and will be incorporated into a future, more advanced device.

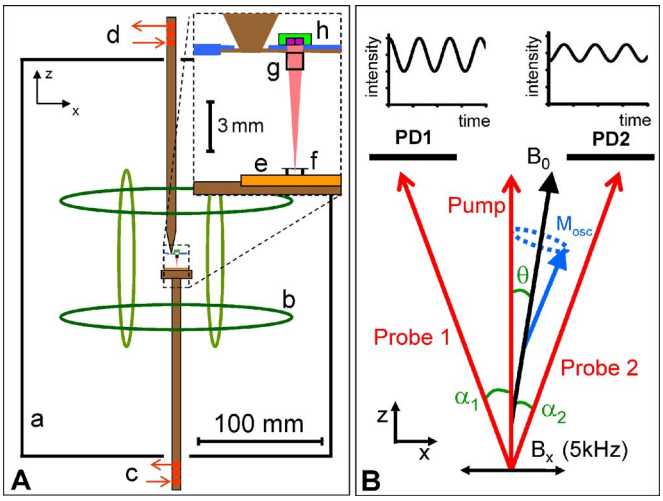

FIG. 1. (Color online) (A) Diverging beam magnetometer. (a) Single-layer magnetic shield. (b) Three-dimensional Helmholtz coils. [(c) and (d)] Heating coils for laser and cell "hot fingers." (e) VCSEL baseplate. (f) VCSEL with quarter wave plate on top. (g) ^{87}Rb cell. (h) Quadrant photodiode. (B) A schematic diagram of the operation of the differential magnetometer. The average direction of the pump beam defines the z axis. $\mathbf{B_0}$ is the field to be measured, lying at an angle θ to the z axis. θ=0 for optimal differential signal.

[a]Electronic mail: hodby@boulder.nist.gov

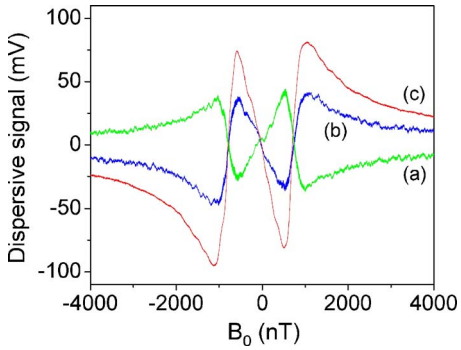

FIG. 2. (Color online) Output of the lock-in amplifier, referenced to the 5 kHz driving field as $\mathbf{B_0}$ is slowly scanned with $\theta=0$. (a) photodiode 1, (b) photodiode 2, and (c) differential signal.

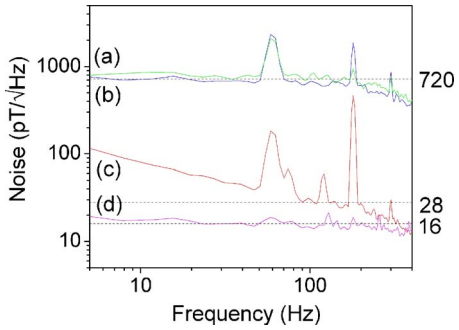

FIG. 3. (Color online) Noise at the zero crossing of the 700 nT dispersive resonance (Fig. 2) as a function of frequency. (a) photodiode 1 only, (b) photodiode 2 only, (c) differential signal, and (d) technical and fundamental noise limit—measured electronic noise (including johnson noise) with calculated photon shot noise added in quadrature. A measurement of the noise on each channel around 100 Hz is taken and displayed on the right hand axis.

A schematic diagram showing the operation of the differential magnetometer is shown in Fig. 1(b). The aim is to measure the Larmor frequency associated with the magnetic field $\mathbf{B_0}$ and hence the magnitude of $\mathbf{B_0}$. The Larmor precession rate ω_0 is given by $\omega_0=2\pi\gamma B_0$, where γ is the gyromagnetic ratio of ^{87}Rb (7 Hz/nT). The strong, central part of the circularly polarized laser beam is primarily responsible for optically pumping ^{87}Rb atoms into the $|F=2,m_F=2\rangle$ level of the $5S_{1/2}$ ground state, creating a net atomic spin in the $\hat{z}$ direction.[9] Spin precession around $\mathbf{B_0}$ is coherently driven by the oscillating field $B_x=B_1\cos\omega t$, where $B_1=0.19$ μT and $\omega=2\pi\times5$ kHz. The magnitude of $\mathbf{B_0}$ is scanned at 37.4 nT/ms. A resonant response occurs when the frequency of the Larmor precession around B_0 matches the driving frequency ω, creating a spin precession of large amplitude (M_{osc}). The component of this precessing spin that lies along the ith probe beam (M_i) determines the absorption of the beam and hence the light intensity reaching the ith photodiode. Passing the output of the ith photodiode through a lock-in amplifier referenced to the driving field B_x enables us to extract the phase and amplitude of the oscillatory part of M_i. In a practical magnetometry application we would scan the driving frequency rather than the amplitude of $\mathbf{B_0}$ to find the resonance, but for demonstrating the principle of the magnetometer, either method is suitable.

A full description of the behavior of the driven spin system can be derived from Bloch's equations.[10] They may be simplified in our experiment to give the following expression for the phase and amplitude of the oscillatory part of M_i:[11]

$$M_i \propto \cos^2\theta\sin(\theta-\alpha_i)\left[\frac{1}{T_2}\left(\frac{1}{1/T_2^2+(\omega_0-\omega)^2}\right)\sin\omega t - \left(\frac{\omega_0-\omega}{1/T_2^2+(\omega_0-\omega)^2}\right)\cos\omega t\right], \quad (1)$$

where θ is the average angle between the pump beam and $\mathbf{B_0}$ (set to zero for the first part of this letter) and α_i is the average angle between the pump beam and the ith probe beam. The second term in this familiar resonance expression is dispersionlike and ideally suited for a magnetometer output signal (Fig. 2). This expression ignores the effects of transverse optical pumping by the probe beams which is justified by our use of the normal Gaussian angular intensity distribution of the light emitted by the laser.

An important figure of merit for a magnetometer is its sensitivity, or the smallest change in field that it can detect for a given bandwidth. This is determined by looking at the voltage noise around the zero crossing of the magnetometer signal and using the signal gradient to convert this to a field uncertainty. Noise measurements for the two individual photodiodes are shown in Figs. 3(a) and 3(b). These single-channel magnetometers have a sensitivity of 720 pT/$\sqrt{\mathrm{Hz}}$ at 100 Hz.

If the dominant noise on these single-channel magnetometers is common to both photodiodes (e.g., laser amplitude noise or frequency noise converted to amplitude noise by the atomic absorption profile[12]), it can be removed by subtracting the two photodiode signals before they enter the lock-in amplifier. The rejection ratio was optimized to a value of 1:1000 by applying a 5 kHz modulation to the laser current and minimizing the differential signal. The relative size and phase of the signals are also affected by bias field offsets that alter the plane of precession of the atomic spins and hence the size and phase (relative to the driving field) of the spin component parallel to each probe beam. Once the electronics had been adjusted to optimize noise rejection, careful field nulling was required to achieve the symmetric, equally sized signals seen on each channel in Figs. 2(a) and 2(b).

While common-mode noise on each photodiode has the same sign and is subtracted, the signals have opposite sign [provided $|\theta|<|\alpha_i|$ and $\mathbf{B_0}$ lies between the two photodiodes—see Eq. (1)] and hence are added, further improving the signal-to-noise ratio of the differential magnetometer. The differential signal is shown in Fig. 2(c) and is approximately twice the size of the individual photodiode signals. The noise spectrum for the differential magnetometer is shown in Fig. 3(c). It has a sensitivity of 28 pT/$\sqrt{\mathrm{Hz}}$ at 100 Hz, improving on the single-channel magnetometer by a factor of 26. It is within a factor of 2 of the measured technical and fundamental noise floor of the instrument [Fig. 3(d)], which is due to technical electrical noise, Johnson noise, and photon shot noise in roughly equal amounts.

We also investigated if the signal size and hence the sensitivity might be improved further by allowing $\mathbf{B_0}$ to tilt in the XZ plane. The angular dependence of Eq. (1) can be explained by looking at the origin of each of the cosine and sine terms. Optical pumping efficiency accounts for one factor of $\cos\theta$, and the component of $\mathbf{B_x}$ able to drive the spin precession around $\mathbf{B_0}$ accounts for the second. The term $\sin(\theta-\alpha_i)$ comes from the amplitude of the precessing spin

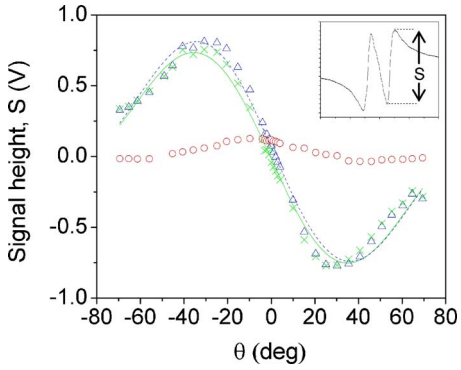

FIG. 4. (Color online) Dispersion signal height (S) as a function of the tilt angle of $\mathbf{B_0}$, θ. Photodiode 1 only (crosses, solid line), photodiode 2 only (triangle, dotted line), and differential signal (circles). The symbols show experimental data and the lines show a fit of the θ dependence of Eq. (1) to the data.

component that lies along the ith probe beam (M_i) and modulates the beam transmission.

In Fig. 4, the angular dependence of Eq. (1) is fitted to experimental plots of signal size versus θ for each photodiode and shows excellent agreement. The zero-amplitude points occur when $\theta=\alpha_i$ and $\mathbf{B_0}$ is pointing directly at one photodiode, causing the atomic spins to precess in a plane perpendicular to the corresponding probe beam. The separation of these zero-amplitude points enables us to measure the "effective divergence angle" of the laser beam, $2|\alpha_i|$. Due to the finite area of the photodiode, defects in the cell windows, and unknown clipping of the beam, we can make only a rough estimate of this quantity from the apparatus geometry, $2|\alpha_i|<7°$. The experimental separation in Fig. 4 is 2.4(9)°, in good agreement with our theoretical estimate. On the same plot we also show the differential signal size as a function of tilt angle (open circles). This has a maximum at $\theta=0$, when the signals from each channel have opposite sign and hence add constructively in the subtractor. When $|\theta|>|\alpha_i|$ and $\mathbf{B_0}$ lies outside the angular range of the photodiodes, the individual signals have the same sign and tend to cancel. The experimental data are in good agreement with theory.

While $\theta=0$ will always be optimal for the differential design, the signal size can be improved by up to a factor of 48 if the angle of the probing part of the beam, $|\alpha|$, is increased from its current value of 1.2° to 90°; the sensitivity is expected to increase accordingly. Construction has begun on two new magnetometer designs which take advantage of this.

In summary, we have demonstrated a miniature differential magnetometer physics package using a novel diverging beam design, well suited to wafer-level mass production of chip-scale devices. Differential operation of the magnetometer is shown to improve the sensitivity by a factor of 26 over an equivalent single-channel device. We have also evaluated design improvements that will improve the sensitivity further without sacrificing the simplicity or miniature size of the current device.

The authors gratefully acknowledge advice and technical support from P. Schwindt, S. Knappe, S. Schima, and N. Copeland. This work was supported by the Microsystems Technology Office of the U.S. Defense Advanced Research Projects Agency (DARPA).

[1] J. Clarke, *SQUID Sensors: Fundamentals, Fabrication and Applications* (Kluwer Academic, Dordrecht, The Netherlands, 1996).
[2] D. Budker and M. V. Romalis, Nat. Phys. **3**, 227 (2007).
[3] I. K. Kominis, T. W. Kornack, J. C. Allred, and M. V. Romalis, Nature (London) **422**, 596 (2003).
[4] P. Schwindt, B. Lindseth, S. Knappe, V. Shah, and J. Kitching, Appl. Phys. Lett. **90**, 081102 (2007).
[5] H. Xia, A. Ben-Amar Baranga, D. Hoffman, and M. V. Romalis, Appl. Phys. Lett. **89**, 211104 (2006).
[6] W. H. Farthing and W. C. Folz, Rev. Sci. Instrum. **38**, 1023 (1967).
[7] S. Knappe, V. Shah, P. Schwindt, L. Hollberg, J. Kitching, L.-A. Liew, and J. Moreland, Appl. Phys. Lett. **85**, 1460 (2004).
[8] L.-A. Liew, S. Knappe, J. Moreland, H. Robinson, L. Hollberg, and J. Kitching, Appl. Phys. Lett. **84**, 2694 (2004).
[9] Despite the high buffer gas pressure, collision with the walls of this miniature cell is still the dominant decoherence mechanism, showing that the Rb atoms diffuse a significant distance before they lose coherence. Thus, while some additional pumping will occur in the wings of the beam, the primary process in this magnetometer involves pumping near the center of the beam where the intensity is strongest, followed by diffusion outwards to be probed.
[10] F. Bloch, Phys. Rev. **70**, 460 (1946).
[11] A. Bloom, Appl. Opt. **1**, 61 (1962).
[12] J. C. Camparo and J. G. Coffer, Phys. Rev. A **59**, 728 (1999).